NJC

PAPER

View Article Online
View Journal | View Issue

Cite this: *New J. Chem.*, 2014, **38**, 2386

Two novel aggregation-induced emission active coumarin-based Schiff bases and their applications in cell imaging†

Hongde Xiao,[a] Kun Chen,[a] Dandan Cui,[b] Nannan Jiang,[b] Gui Yin,*[ac] Jie Wang[a] and Ruiyong Wang*[b]

Received (in Montpellier, France) 11th December 2013,
Accepted 28th January 2014

DOI: 10.1039/c3nj01557b

www.rsc.org/njc

Two new coumarin-based Schiff bases, 8,8′-((1*E*,1′*E*)-hydrazine-1,2-diylidenebis(methanylylidene))bis-(7-hydroxy-4-methyl-2*H*-chromen-2-one), (CHC), and 7-hydroxy-8-((*E*)-((*E*)-((2-hydroxynaphthalen-1-yl)-methylene)hydrazono)methyl)-4-methyl-2*H*-chromen-2-one, (CHN), with excited-state intramolecular proton-transfer (ESIPT) properties, were synthesized and characterized. Both of the compounds displayed aggregation-induced emission (AIE) characteristics, of which CHC nanoparticles emitted a reddish orange fluorescence, while the CHN nanoparticles exhibited a saffron yellow fluorescence. The appearance of emission peaks in the long wave regions with large Stokes-shifts demonstrated the occurrence of the ESIPT process. Observations of the nanoparticles' morphologies were undertaken through a transmission electron microscope (TEM) method. Furthermore, due to the good biocompatibilities, high stabilities and the large Stokes-shifts, the two compounds were ideal candidates for cell staining.

Introduction

Over the past few decades, efficient organic fluorescent materials have been attracting considerable research interest due to their potential applications, including in organic light-emitting diodes (OLED),[1] organic field effect transistors (OFET),[2] fluorescent sensors,[3] photovoltaic cells,[4] fluorescent biological labels,[5] organic lasers,[6] *etc.* Although many traditional organic fluorophores with large delocalized π-conjugated moieties emit strongly in their dilute solutions, the emissions become weak at high concentrations or in aggregated states,[7] which is known as concentration quenching or aggregation-caused quenching (ACQ). The reason for this is believed to be because the excited states of the aggregates often decay *via* non-radiative pathways caused by strong intermolecular vibronic interactions, such as exciton coupling and excimer formation in the solid state.[8] The notorious ACQ effect has greatly limited the efficiency of organic fluorescent materials because in practice, those materials are commonly used in the solid state. Various approaches, such as encapsulation by amphiphilic surfactants and blending with transparent polymers,[9] have been undertaken to prevent the aggregation but have been met with only limited success.

Fortunately, materials displaying aggregation-induced emission (AIE) characteristics can be used to tackle this problem. Since the first AIE compound, 1-methyl-1,2,3,4,5-pentaphenylsiole, was synthesized by Tang's group,[10] several organic compounds based on different fluorophores have been reported to display AIE characteristics, such as 1-cyano-*trans*-1,2-bis-(4′-methylbiphenyl)ethylene (CN-MBE),[11] diphenyldibenzofulvene (DPDBF) derivatives,[12] rhodanineacetic acid-pyrene derivative (RAAP),[13] whose potential applications were further investigated in the fields of bio/chem sensors,[14] cell imaging[15] and optoelectronic devices.[16]

In recent years, a few interpretations of AIE in terms of the intra- and intermolecular effects have been reported. Intramolecular effects on fluorescence enhancement are simply explained by the conformational changes from the twisted conformations to the planar ones. The planar conformations are favourable for the radiation process.[17] Intermolecular interactions are related with the specific aggregation morphology (H-type and J-type aggregation). H-aggregates tend to induce the nonradiative deactivation process, where as J-aggregates induce a relatively high fluorescence efficiency.[18]

As far as the specific emission properties are concerned, the excited-state intramolecular proton-transfer (ESIPT) process could greatly contribute to the fluorescent emission of the chromophore in the solid state. The planar conformations are

[a] *State Key Laboratory of Analytical Chemistry for Life Science, School of Chemistry and Chemical Engineering, Nanjing University, Nanjing 210093, People's Republic of China. E-mail: yingui@nju.edu.cn*
[b] *School of Life Science, Nanjing University, Nanjing, 210093, People's Republic of China. E-mail: wangry@nju.edu.cn*
[c] *Jiangsu Key Laboratory of Advanced Catalytic Materials and Technology, Changzhou University, 213164, China*

† Electronic supplementary information (ESI) available. See DOI: 10.1039/c3nj01557b

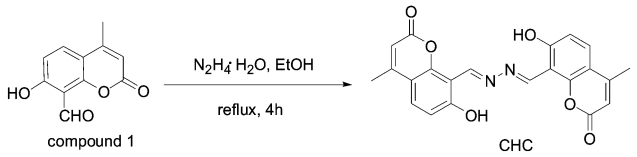

Scheme 1 Synthesis of CHC.

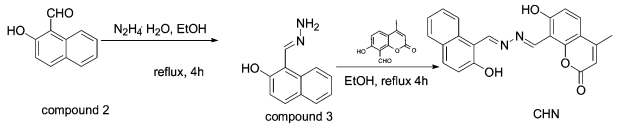

Scheme 2 Synthesis of CHN.

beneficial to both AIE and ESIPT. The ESIPT dyes can present a large Stokes shift caused by transformation of the excited enol form (E*) to the excited proton-transferred keto form (K*), diminishing the self-absorption to a great extent. This property enables the ESIPT compounds to have a wide range of applications in systems such as fluorescent probes,[19] laser dyes,[20] organic electroluminescence optical materials,[21] scintillators,[22] as well as in solar collectors.[23]

In general, an ESIPT mechanism involves a proton transfer from the donor to the acceptor moiety.[24] The most common ESIPT donor is the phenolic OH, and the basic group is usually a heteroatom, such as carbonyl oxygen or a nitrogen atom on amide. In terms of the structures of AIE compounds, the molecules have been found to be associated with aromatic groups with rotatable C–C, C–N or N–N single bonds.[25] Due to the superior light stability, high fluorescent quantum yield, as well as the good biocompatibility, coumarin derivatives have become ideal candidates for fluorescent biological materials. These factors motivated us to design and synthesize two novel coumarin-based ESIPT compounds, 8,8′-((1*E*,1*E*′)-hydrazine-1,2-diylidenebis(methanylylidene))bis(7-hydroxy-4-methyl-2*H*-chromen-2-one), (CHC, Scheme 1), and 7-hydroxy-8-((*E*)-((*E*)-((2-hydroxynaphthalen-1-yl)methylene)hydrazono)methyl)-4-methyl-2*H*-chromen-2-one, (CHN, Scheme 2). In addition, their nanoparticles were prepared by a simple reprecipitation method without using surfactants. What is more, the biocompatibility and the cell uptake behavior of the nanoparticles were investigated to evaluate their potential applications in cell imaging.

Experimental

Reagents, materials and equipment

All reagents were of analytical grade unless otherwise stated. ^{1}H-NMR spectra were recorded on Bruker Ultrashield 300 MHz NMR spectrometer. Chemical shifts were expressed in ppm (in DMSO-d_6 or $CDCl_3$; TMS as an internal standard) and coupling constants (*J*) in Hz. Mass spectroscopy was obtained from a Thermo LCQ Fleet MS spectrometer in negative ion mode. Differential scanning calorimetry (DSC) and thermal gravimetric analysis (TGA) were investigated on a Netzsch STA 449 C. UV-vis absorption and fluorescence spectra were measured using a Perkin Elmer Lambda 35 spectrophotometer and Perkin Elmer LS-55 spectrophotometer, respectively. Transmission electron microscopy (TEM) images were recorded on a JEX-2100 transmission electron microscope. Fluorescence microscope photographs of the nanoparticles and cell imaging were captured by n Olympus FV-1000 laser scanning confocal fluorescence microscope.

Synthesis of compound 2

Compound **2** was synthesized according to our previous procedure.[26]

Synthesis of 7-hydroxy-4-methyl-coumarin

4-Methylbenzenesulfonic acid (5 g) was added to a solution of resorcinol (11.0 g, 0.1 mol) in toluene (40 mL), and then acetoacetic ester (13.0 g) was added drop wise. The reaction mixture was refluxed for 3 h and monitored by TLC until the resorcinol was completely consumed. After cooling, the solution was poured into ice water (100 mL), a yellow precipitate was collected by filtration and washed with cold water. A pale yellow solid was obtained by recrystallization with 95% ethanol (11.3 g, yield: 64%). M.p. 185.0–186.0 °C. ^{1}H NMR (300 MHz, CD_3OD), δ = 7.61 (d, 1H, *J* = 8.9 Hz), 6.83 (d, 1H, *J* = 10 Hz), 6.70 (s, 1H), 6.10 (s, 1H), 2.42 (s, 3H). TOF MS EI calcd 176.0, found 176.0.

Synthesis of compound 1[27]

7-Hydroxy-4-methyl-coumarin (5.3 g, 0.03 mol) and hexamine (9.8 g, 0.07 mol) in glacial acetic acid (50 mL) were refluxed for 5.5 h, and then 20% HCl (75 mL) was added and the solution was heated for 1 h. After cooling, the reaction mixture was extracted with ether, and the combined organic layers were evaporated under reduced pressure. The residue was poured into ice water, and a pale yellow solid of 8-formyl-7-hydroxy-4-methyl-coumarin was obtained. Further purification was carried out by recrystallization with hot ethanol to obtain a light yellow powder (612.1 mg, yield: 10%). M.p. 180–181.0 °C (lit. 120.0–122.0 °C). ^{1}H NMR (300 MHz, $CDCl_3$): δ = 12.22 (s, 1H); 10.62 (s, 1H); 7.74 (d, 1H, *J* = 9 Hz); 6.92 (d, 1H, *J* = 9 Hz); 6.21 (s, 1H); 2.43 (s, 3H). TOF MS EI calcd 204.0, found 204.0.

Synthesis of CHC

8-Formyl-7-hydroxy-4-methyl-coumarin (408 mg, 2 mmol) was added to a solution of aqueous hydrazine (85%, 0.1 mL, about 2 mmol) in methanol (20 mL). Then the mixture was refluxed for 4 h. After completion of the reaction, the obtained yellow precipitate was filtered and washed several times with cold ethanol to give CHC (347 mg) as a pure yellow solid in 86% yield. ^{1}H NMR (300 MHz, DMSO-d_6): δ = 12.78 (s, 1H), 8.40 (s, 1H), 7.54 (d, *J* = 9.0 Hz, 1H), 6.87 (d, *J* = 9.0 Hz, 1H), 6.19 (s, 1H), 2.38 (s, 3H); ^{13}C NMR (75 MHz, DMSO-d_6) δ 160.69, 160.01, 154.43, 151.21, 135.49, 125.67, 113.33, 112.13, 110.85, 107.22, 18.80. ESI-HRMS: calcd for $(C_{22}H_{16}N_2O_6 - H)^-$ *m*/*z* 403.0930, found $(M - H)^-$: 403.0791.

Synthesis of CHN

A solution of 1-(hydrazonomethyl)naphthalene-2-ol (**2**) (186 mg, 1 mmol) and 7-hydroxy-4-methyl-2-oxo-2*H*-chromene-8-carbaldehyde (204 mg, 1 mmol) in 20 mL of ethanol was refluxed for 4 h. After completion of the reaction, the obtained yellow precipitate was filtered and washed several times with cold ethanol to give CHN (346 mg) as a pure yellowish solid in 93% yield. ^{1}H NMR (300 MHz, DMSO-d_6) δ 12.54 (s, 1H), 12.51 (s, 1H), 9.96 (s, 1H), 9.34 (s, 1H), 8.65 (d, J = 8.5 Hz, 1H), 8.02 (d, J = 9.0 Hz, 1H), 7.89 (d, J = 7.8 Hz, 1H), 7.78 (d, J = 9.0 Hz, 1H), 7.60 (t, J = 7.5 Hz, 1H), 7.42 (t, J = 7.5 Hz, 1H), 7.24 (d, J = 9.0 Hz, 1H), 7.01 (d, J = 8.9 Hz, 1H), 6.26 (s, 1H), 2.39 (s, 2H); ^{13}C NMR (126 MHz, DMSO-d_6) δ 163.58, 162.61, 160.94, 159.58, 158.06, 154.31, 135.80, 133.49, 132.83, 130.42, 129.41, 128.65, 128.37, 124.39, 122.54, 119.24, 114.03, 112.48, 111.37, 108.88, 105.98, 518.80; ESI-HRMS: calcd for $(C_{22}H_{16}N_2O_4 - H)^-$ m/z 372.1032, found $(M - H)^-$: 371.2560.

Preparation of the samples

Preparation of the nanoparticles. CHC or CHN DMSO solutions (10 μL, 1 × 10^{-3} M) were rapidly injected into 2 mL of DMSO–H_2O mixtures of different ratios, respectively, with vigorous stirring at room temperature. The nanoparticles, with both having concentrations of 5 μM (represented by the concentration of monomer, and it means the same hereinafter), were taken for fluorescence emission spectra and UV-visible absorption respectively.

Preparation of the samples for TEM images. The nanoparticles were deposited on a 300-mesh copper grid coated with carbon, and observed at an accelerating voltage of 200 kV at room temperature.

Preparation of the samples for fluorescence microscope images. A drop of the CHC or CHN nanoparticle suspension was dropped onto a glass slide, and then covered with a coverslip. The excitation wavelength was set at 405 nm, with the choice of suitable filters.

Cell culture

HeLa cells were cultured in Dulbecco's modified Eagle's medium (DMEM) containing 10% fetal bovine serum and antibiotics (100 units mL^{-1} penicillin and 100 μg mL^{-1} streptomycin), and maintained at 37 °C in a humidified atmosphere of 95% air and 5% CO_2.

Cell imaging

A fresh stock of HeLa cells was seeded into a glass bottom dish with a density of 1 × 10^{-5} cells per dish, and incubated for 24 h. Subsequently, the cells were incubated with 5 μM CHC or CHN nanoparticles in DMEM solution (adding 100 μL 10^{-3} M DMSO concentrated solution CHC or CHN to 1900 μL DMEM) for 4 h at 37 °C. Afterwards, the cells were washed three times with PBS to remove any nanoparticles attached to the surface of cells and then fixed with 4% paraformaldehyde for 10 min at room temperature. The cells were imaged under a confocal laser scanning microscope (Olympus, FV-1000; λ_{ex} = 405 nm; fluorescent signals were collected at 420–700 nm for CHC and 430–650 nm for CHN). The images were captured using a photomultiplier.

Results and discussion

Both CHC and CHN were soluble in common organic solvents, but insoluble in water. Hence, we employed a simple reprecipitation method without surfactants to obtain the CHC and CHN nanoparticles. The molecularly dissolved dilute DMSO solutions of CHC and CHN were transparent, emitting very weak fluorescence, which could hardly be observed (left of the two inert pictures of Fig. 1). After the addition of water, as the nanoparticles formed, the reddish orange fluorescence of the CHC nanoparticles (middle and right of Fig. 1a) and the saffron yellow fluorescence (middle and right of Fig. 1b) of the CHN nanoparticles could be observed by the naked-eye. The molar absorptivities for these two compounds as aggregates were 2.77 × 10^4 (CHC, λ_{ex} = 335 nm) and 2.14 × 10^4 (CHN, λ_{ex} = 340 nm). The nanoparticle suspensions were transparent without precipitation and were observed to be stable even after a month.

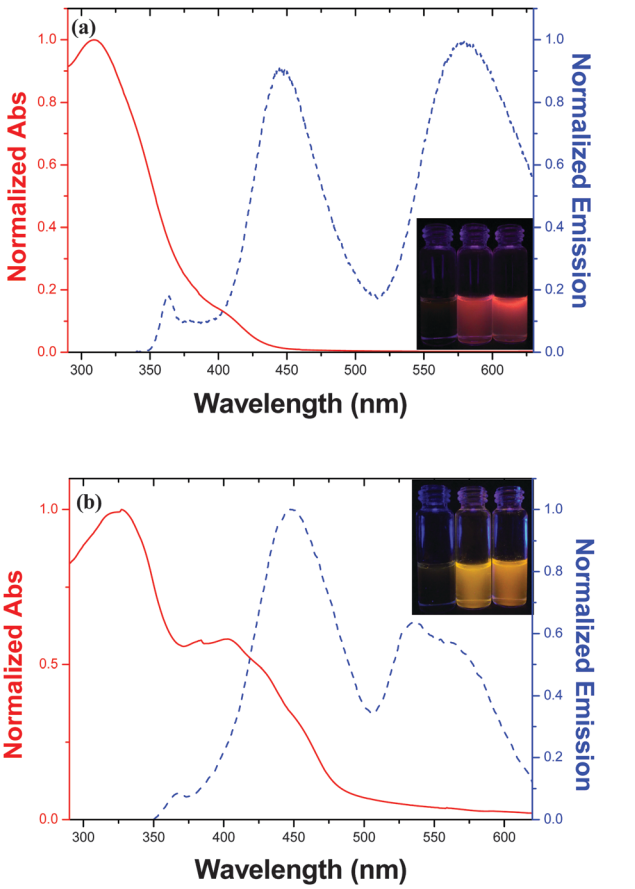

Fig. 1 Normalized absorption (solid line) and emission (dashed line) spectra of CHC nanoparticles in the water/DMSO (v/v, 9/1) mixture (a) and CHN nanoparticles in he water/DMSO (v/v, 7/3) mixture (b). Inert: photographs of CHC (a) and CHN (b) both with concentrations of 5 × 10^{-5} M in DMSO dilute solution (left) and in water/DMSO mixtures (middle, v/v, 1/1; right, v/v, 9/1) under 365 nm irradiation.

As shown in the normalized absorption and emission spectra of the CHC nanoparticles and CHN nanoparticles, large stokes shifts of ~270 nm for the CHC nanoparticles and ~240 nm for the CHN nanoparticles could be detected. Moreover, the quantum yield of the CHC (as aggregates) was 0.827 and the quantum yield of CHN (as aggregates) was 0.546, (using quinine as the reference with a known Φ value of 0.577 in 0.05 M H_2SO_4), indicating the great properties of CHC and CHN acting as solid state light-emitting materials.

Thermal stability tests

The thermal stabilities of CHC and CHN were investigated by differential scanning calorimetry (DSC) and thermal gravimetric analysis (TGA). Fig. 2 showed that the decomposition temperatures of CHC and CHN were both over 300 °C, demonstrating their thermally stability.

Observation of the CHC and CHN nanoparticles

TEM observation. The transmission electron microscope (TEM) images were obtained to observe the shape and size of the nanoparticles. The TEM image in Fig. 3a showed that the CHC nanoparticles were claviform particles with a mean length of 500 nm. While, as shown in Fig. 3b, the CHN nanoparticles were fine spheres with diameters ranging from 60 to 100 nm.

Fluorescence microscope images. The fluorescence microscope images of CHC and CHN are shown in Fig. 4a and b. Upon excitation at 405 nm, the CHC nanoparticles emitted a reddish orange fluorescence, and the observed claviform shape fits with the TEM observation. In addition, for CHN, a large

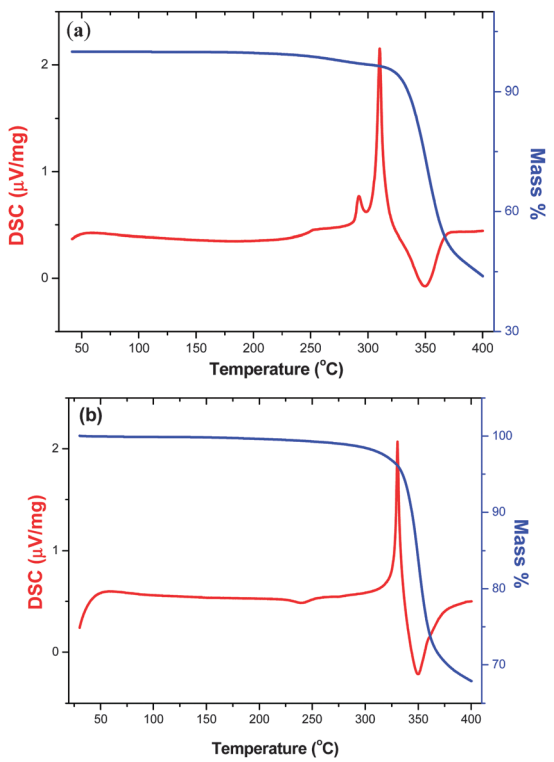

Fig. 2 DSC and TG curves of CHC (a) and CHN (b).

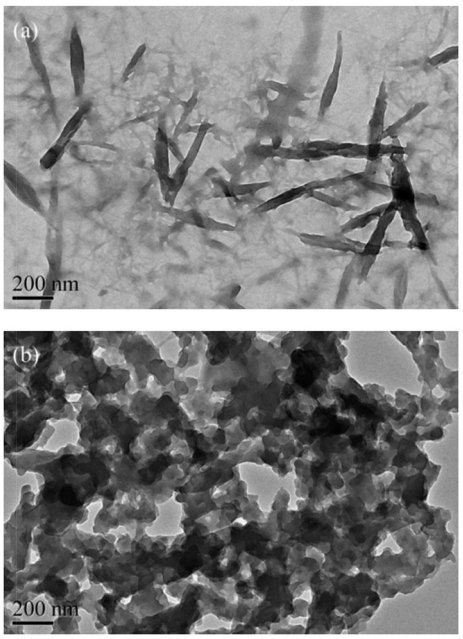

Fig. 3 Transmission electron microscope (TEM) images of CHC (a) and CHN (b) nanoparticles obtained from suspensions of the water–DMSO mixture.

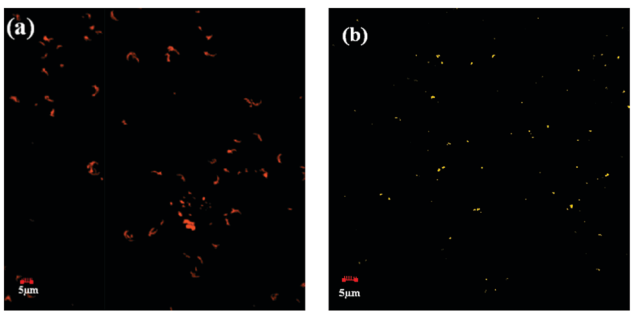

Fig. 4 Fluorescence microscope images of CHC (a) and CHN (b) nanoparticles (water/DMSO = 7/3, v/v).

number of fluorescent dots emitting light could be observed. Also, the mean length of the CHC fluorescent bodies was 3 μm, and the diameter of CHC fluorescent bodies was 1 μm. Both were larger than the sizes observed by TEM which could be ascribed to the diffusion of light. Accordingly, the mutual authentication of fluorescent images and the TEM images confirmed the existence of the CHC and CHN particles further.

Aggregation-induced emission phenomenon

The fluorescence spectra of the CHN nanoparticles in the water–DMSO mixtures with various ratios (keeping the concentration 5×10^{-6} M) upon excitation at 323 nm and 416 nm are shown in Fig. 5, respectively. As for the excitation at 323 nm, CHN in DMSO solution without water showed two weak peaks at 392 and 529 nm. In this situation, the CHN molecules existed in the isolated state. Because of the free rotations of the C–N single bonds, the ground state molecules could form a board range of torsional angles, from planer to twisted. So, in this

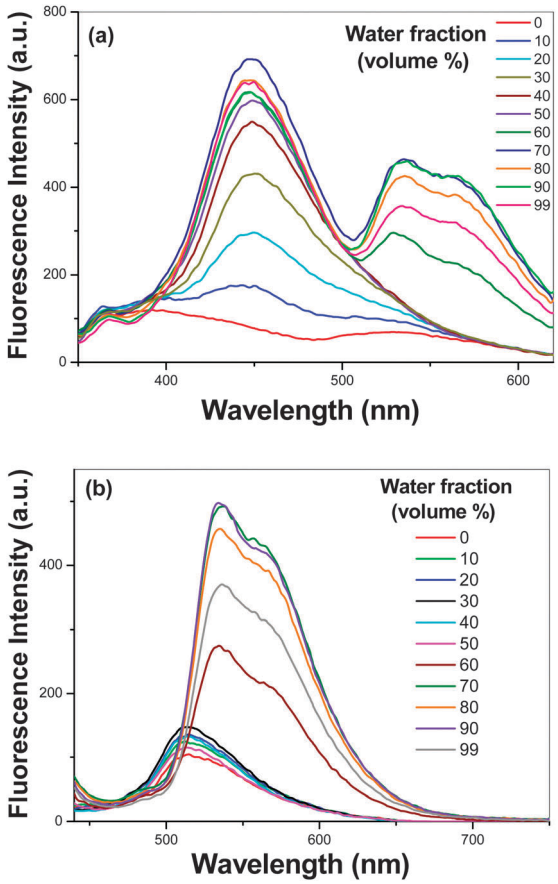

Fig. 5 Fluorescent spectra changes of CHN (5×10^{-6} M) depending on the volume fraction of water in DMSO, λ_{ex} = 323 nm (a) and λ_{ex} = 416 nm (b).

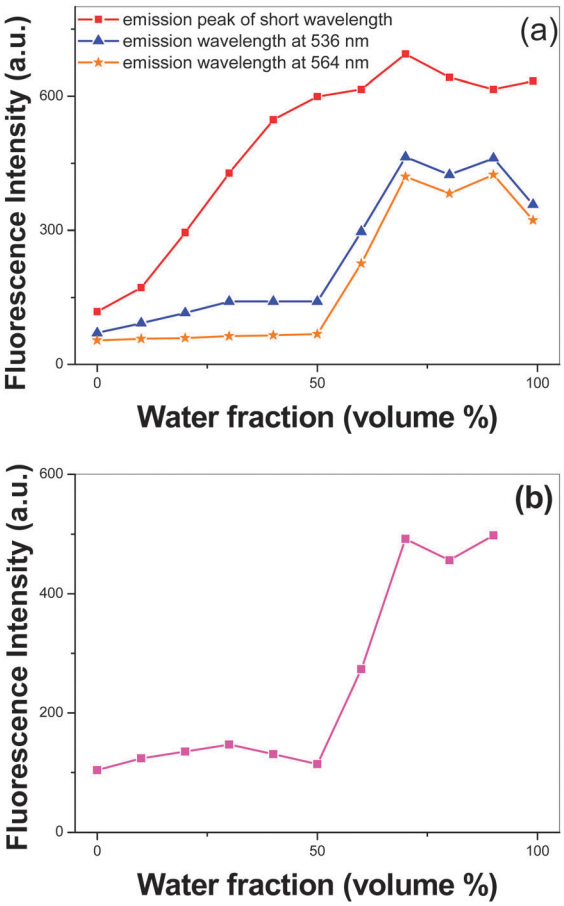

Fig. 6 Variation in the fluorescence intensity of different emission peaks for CHN with the increasing volume fraction of water in DMSO, λ_{ex} = 323 nm (a) and λ_{ex} = 416 nm (b).

state we expected to have no emission due to the nonradiative decay processes brought about through the molecular torsions and rotations.[17] However, different from the hypothetical conditions, in the actual excited state, the existence of hydrogen bonds to some extent hinders the free rotations. What is more, the relatively high viscosity of the DMSO solution also attributes to the restriction of intramolecular rotation (RIR).[28] As a result, a weak and broad emission is formed due to the restriction of intramolecular rotation, the enhancement of planarity, and the improvement of conjugation.

As the water fraction increased, a new emission peak located at 447 nm appeared. The fluorescence intensity enhanced gradually namely the AIE characteristic of CHN, indicating the formation of aggregated nanoparticles. This enhancement was depicted in Fig. 6a. In the long wavelength region, when the fraction of water increased to 60%, an emission peak located at 534 nm appeared, with a shoulder emission peak at 565 nm. The fluorescent intensity values of the three peaks all reached a maximum (Φ_F = 0.546) in the presence of 70% water.

The enhanced fluorescence emission could be explained in terms of intra- and intermolecular effects. The CHN molecule consists of an N–N moiety as a bridging group. Rather than there being free rotation in the isolated state, a more planar conformation was favored in the aggregation state. Hence the nonradiative decay could be prevented. Therefore, the conformational changes relating to the rotation of the N–N moiety played an important role on the AIE.

In addition, it was probable that the aggregation-induced planarizations inevitably induced the intermolecular interactions. It is widely acknowledged that the formation of an excimer complex, which can be ascribed to the strong intermolecular interactions of planar π-conjugated in the solid state, leads to fluorescence quenching.[8] However, in CHN the bulky and polar hydroxy group restricts the parallel face-to-face intermolecular interactions in the aggregated state, namely the H-aggregate formation which exhibits blue-shifted absorption bands compared to the isolated state.[17] The prevention of H-aggregation forces the head-to-tail aggregation, the J-aggregation, which induces a great enhancement in the fluorescence. The absorption spectra of CHN in the isolated state and aggregated state, shown in Fig. S1 (ESI†), were also in accordance with the bathochromic shift in the absorption maximum of J-aggregation.

Therefore, most probably, the fluorescent enhancement of CHN could be ascribed to the combined effects of aggregation-induced planarization and J-aggregate formation.

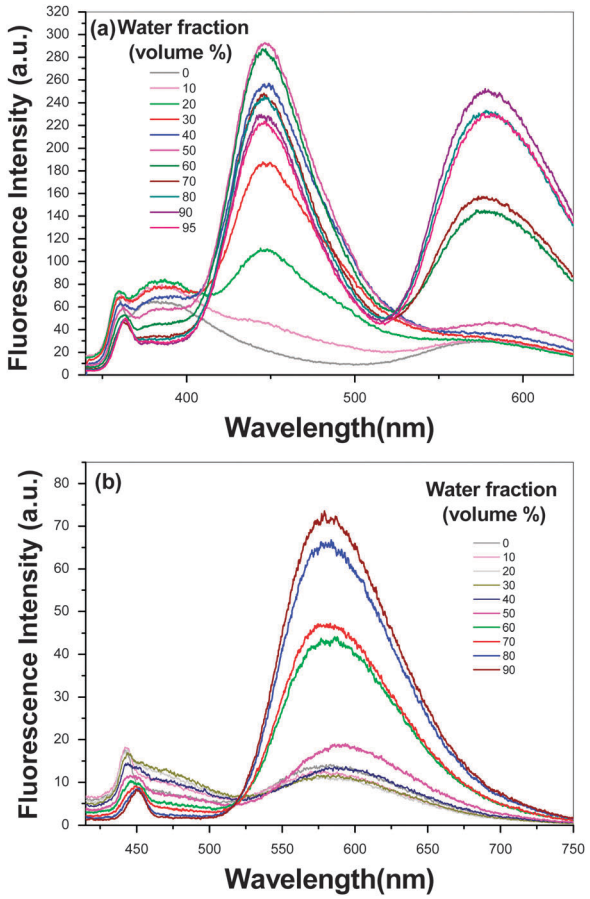

Fig. 7 Fluorescent spectra changes of CHC (5×10^{-6} M) depending on the volume fraction of water in DMSO, λ_{ex} = 323 nm (a) and λ_{ex} = 390 nm (b).

After the water fraction increased to 70%, the fluorescence intensities decreased with further increases of the water fraction. This emission decrease could be explained by the change in the shapes of the aggregates. When the water fraction was lower than 70%, the molecules accumulate slowly in an ordered way to form more emissive nanoparticles.[12] Whereas in a system with a higher water fraction, the CHN molecules agglomerated quickly in a random way to form amorphous nanoparticles that were less emissive. Concerning the emission spectra upon excitation at 416 nm shown in Fig. 5b, the conditions were similar to excitation at 323 nm for the long wavelength region. However, no emission peak in the short wavelength region could be observed. As for the CHC nanoparticles, the conditions were similar except for the specific water fractions, and they are depicted in Fig. 7.

Investigation of the contribution of ESIPT to fluorescent emission features

In order to verify whether proton-transfer exists and how it impacts the excited state of CHC and CHN, we measured the FL spectra in solvents with different polarities. At the same concentration, we noticed that the emission intensities decreased with the increase of the polarity of the solvent, as shown in Fig. S2 (ESI†), because these two ESIPT compounds

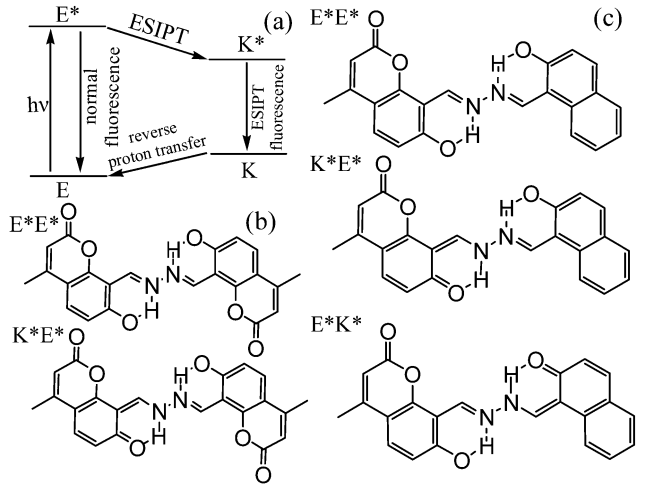

Fig. 8 Mechanism of ESIPT process (a). Excited-state tautomers for CHC (b) and CHN (c).

could form intermolecular H-bonds with protic or polar solvents.[29] Thus, this phenomenon indicated the existence of the ESIPT process to some extent.

The basic process of the ESIPT has been illustrated in the literature,[30] and a brief introduction of ESIPT is shown in Fig. 8a. In the ground state, the enol form (E) was more stable than the keto form (K). Upon photoexcitation, ESIPT occurred on an fs-timescale, transforming the excited enol form (E*) to the excited proton-transferred keto form (K*), which was preferred in the excited state. Then, the excited keto form (K*) relaxed radiatively to the ground-state keto form (K) releasing a large Stokes-shifted fluorescence. Finally, the ground-state keto form (K) transformed to the original enol form (E) in the ground-state.

It is widely acknowledged that ESIPT only occurs through a planar structure because of an increasing ESIPT barrier correlating with the twist angle.[31] On the basis of molecular structure, it had a twisted structure at the energetic minimum of the ground state; while on the other hand, a planar structure was more stable in the excited state. Hence, the transition energy gap of the planar molecules was lower. Therefore, the long wavelength photons, 416 nm for CHN and 390 nm for CHC in our experiment, exclusively excite planar or near-planar molecules, and the proton transfer took place right after excitation leading to no short wavelength region emission being observed. At a short wavelength, 323 nm in our experiment, all molecules were excited. For the planar molecules, the ESIPT process could occur directly. However, for the twisted molecules, the increased barrier enforced the molecules to planarize first before proton-transfer. Therefore, the fluorescence spectra are closely related to the molecular population and reaction rate of ESIPT.

Concerning our fluorescence spectra of CHN upon excitation at 323 nm, as the water fraction increased, the ratio of planar molecules increased as the nanoparticles form. After the water fraction increases to 60%, the ESIPT emission peak could be observed. Based on the discussion above, nanoparticles of

CHN (namely the planar molecules) were expected to emit three maximum peaks coming from the E*E*, E*K* and K*E* tautomers, respectively. The emission maximum peak at 447 nm, with a small Stokes shift and mirror-image shape, could be ascribed to the radiative decay from the E*E*. As for the two emission maximum peaks in the long wavelength region, the large Stokes shifts indicated they are originated from the E*K* and K*E* tautomers separately. The ESIPT emission peak of the phenolic OH on 2-hydroxy-1-naphthaldehyde to nitrogen atom had been reported to be located at 531 nm.[32] In addition, the fluorescence spectra of the CHC nanoparticles which only had a single ESIPT emission peak coming from the E*K* tautomers are shown in Fig. 7, revealed the ESIPT emission peak of phenolic OH on 8-formyl-7-hydroxy-4-methyl-coumarin to the nitrogen atom appeared at 570 nm. Accordingly, emission peak at 534 nm could be assigned to E*K* species and the other emission peak at 565 nm probably came from K*E* species.

Cell staining

Cell permeability enabled the compounds to enter living cells, hence further intracellular investigations became possible. To test whether CHC and CHN could enter cells and serve as biological fluorescence probes, HeLa cells were incubated with the CHC and CHN nanoparticles and then examined by fluorescence confocal microscopy. As shown in Fig. 9, the HeLa cells incubated with the nanoparticle solution and excited by 405 nm, emitted reddish orange fluorescence due to staining with CHC, and a saffron yellow fluorescence due to staining CHN. The merged image revealed that fluorescence could only be detected inside the HeLa cells instead of in random positions. Therefore, CHC and CHN could be assimilated by HeLa cells and aggregates in their cytoplasm. Moreover, cell morphology remained in good condition after intake of the nanoparticles, indicating the great cytocompatibility of CHC and CHN. The biological imaging tests on the HeLa cells have shown that both CHC and CHN have good photophysical properties and could be good candidates for cell staining, avoiding the impacts of excitation light.

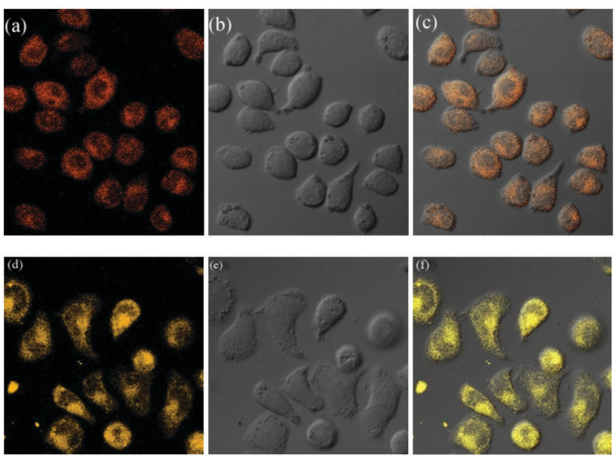

Fig. 9 Confocal microscopy images of cells incubated with 5 μM nanoparticle solution for 4 h, upon excitation at 405 nm. CHC: (a) excited with 405 nm laser. (b) Bright field image. (c) Merged image of (a) and (b). CHN: (d) excited with 405 nm laser. (e) Bright field image. (f) Merged imaged of (d) and (e).

Conclusions

In summary, we have designed and synthesized two coumarin-based fluorescent molecules, CHC and CHN. The two compounds are stable and show high thermal stabilities. In addition, the ESIPT fluorescence could be utilized as a new strategy to develop other AIE-active materials. The success of the coumarin-based series is expected to accelerate organic photo-material discovery and lead to further technological applications in the fields of nanobiotechnology and optoelectronics, and potential uses in cell imaging.

Acknowledgements

This work was supported by the National Basic Research Program of China (No. 2014CB846004) and Jiangsu Key Laboratory of Advanced Catalytic Materials and Technology (No. BM2012110).

Notes and references

1 (*a*) Y. Liu, X. T. Tao, F. Z. Wang, X. N. Dang, D. C. Zou, Y. Ren and M. H. Jiang, *J. Phys. Chem. C*, 2008, **112**, 3975; (*b*) H. Doi, M. Kinoshita, K. Okumoto and Y. Shirota, *Chem. Mater.*, 2003, **15**, 1080; (*c*) C. L. Chiang, M. F. Wu, D. C. Dai, Y. S. Wen, J. K. Wang and C. T. Chem, *Adv. Funct. Mater.*, 2005, **15**, 231.

2 X. G. Yu, J. S. Yu, J. L. Zhou, W. Huang and H. Lin, *Eur. Phys. J.: Appl. Phys.*, 2013, **62**, 20101.

3 (*a*) F. Y. Yan, M. Wang, D. L. Cao, N. Yang, Y. Fu, L. Chen and L. G. Chen, *Dyes Pigm.*, 2013, **98**, 42; (*b*) W. T. Gong, B. Gao, S. Bao, J. W. Ye and G. L. Ning, *J. Inclusion Phenom. Macrocyclic Chem.*, 2012, **72**, 481.

4 H. Anders and G. Michael, *Chem. Rev.*, 1995, **95**, 49.

5 M. Xavier, P. Fabien, L. D. Thilo, D. Maxime, B. P. Marcel, A. A. Paul and W. Shimon, *Single Mol.*, 2001, **2**(4), 261.

6 S. Chénais and S. Forget, *Polym. Int.*, 2012, **61**, 390–406.

7 (*a*) S. A. Jenekhe and J. A. Osaheni, *Science*, 1994, **265**, 765; (*b*) J. Malkin, *Photophysical and Photochemical Properties of Aromatic Compounds*, CRC, Boca Raton, 1992; (*c*) N. J. Turro, *Modern Molecular Photochemistry*, University Science Books, Mill Valley, 1991; (*d*) X. C. Li and S. C. Moratti, in *Photonic Polymer Systems*, ed. D. L. Wise, G. E. Wnek, D. J. Trantolo, T. M. Cooper and J. D. Gresser, Marcel Dekker, New York, 1998, ch. 10.

8 J. B Birks, *Photophysics of Aromatic Molecules*, Wiley, London, 1970.

9 (*a*) W. Z. Yuan, P. Lu, S. M. Chen, J. W. Y. Lam, Z. M. Wang, Y. Liu, H. S. Kwok, Y. G. Ma and B. Z. Tang, *Adv. Mater.*, 2010, **22**, 2159; (*b*) Y. T. Lee, C. L. Chiang and C. T. Chen, *Chem. Commun.*, 2008, 217; (*c*) C. W. Wu, C. M. Tsai and H. C. Lin, *Macromolecules*, 2006, **39**, 4298; (*d*) J. Wang,

Y. F. Zhao, Y. C. Dou, H. Sun, P. Xu, K. Ye, J. Zhang, S. Jiang, F. Li and Y. Wang, *J. Phys. Chem. B*, 2007, **111**, 5082; (*e*) F. He, Y. Tang, S. Wang, Y. Li and D. Zhu, *J. Am. Chem. Soc.*, 2005, **127**, 12343; (*f*) S. Hecht and J. M. J. Frechet, *Angew. Chem., Int. Ed.*, 2001, **40**, 74.

10 J. Luo, Z. Xie, J. W. Y. Lam, L. Cheng, H. Chen, C. Qiu, H. S. Kwok, X. Zhan, Y. Liu, D. Zhu and B. Z. Tang, *Chem. Commun.*, 2001, 1740.

11 (*a*) S. J. Li, B. K. An, S. D. Jung, M. A. Chung and S. Y. Park, *Angew. Chem., Int. Ed.*, 2004, **43**, 6346; (*b*) B. K. An, S. K. Kwon, S. D. Jung and S. Y. Park, *J. Am. Chem. Soc.*, 2002, **124**, 14410.

12 (*a*) H. Tong, Y. Dong, M. Haussler, J. W. Y. Lam, H. H. Y. Sung, I. D. Williams, J. Sun and B. Z. Tang, *Chem. Commun.*, 2006, 1133; (*b*) H. Tong, Y. Dong, Y. Hong, M. Haussler, J. W. Y. Lam, H. H. Y. Sung, X. Sun, J. Yu, I. D. Williams, H. S. Kwok and B. Z. Tang, *J. Phys. Chem. C*, 2007, **111**, 2287.

13 B. Zhang, W. Diao, C. Bi, J. Sun, G. X. Han, Y. Shi, L. Sheng, G. Yin and L. Pu, *J. Fluoresc.*, 2012, **22**, 1.

14 (*a*) Y. Q. Li, R. T. K. Ryan, B. Z. Tang and B. Liu, *RSC Adv.*, 2013, **3**(26), 10135; (*b*) S. Mukherjee and P. Thilagar, *Chem. Commun.*, 2013, **49**, 7292.

15 (*a*) X. Y. Zhang, X. Q. Zhang, B. Yang, M. Y. Liu, W. Y. Liu, Y. W. Chen and Y. Wei, *Polym. Chem.*, 2013, **4**, 4317; (*b*) H. H. Lin, Y. C. Chan, J. W. Chen and C. C. Chang, *J. Mater. Chem.*, 2011, **21**, 3170.

16 A. Hagfeldtt and M. Gratzel, *Chem. Rev.*, 1995, **95**, 49.

17 (*a*) D. Oelkrug, A. Tompert, H. Egelhaaf, M. Hanack, E. Steinhuber, M. Hohloch, H. Meier and U. Stalmach, *Synth. Met.*, 1996, **83**, 231; (*b*) D. Oelkrug, A. Tompert, J. Gierschner, H. Egelhaaf, M. Hanack, M. Hohloch and E. Steinhuber, *J. Phys. Chem. B*, 1998, **102**, 1902; (*c*) M. M. Souza, G. Rumbles, I. R. Gould, H. Amer, I. D. W. Samuel, S. C. Moratti and A. B. Holmes, *Synth. Met.*, 2000, **111–112**, 539.

18 B. K. An, J. Gierschner and S. Y. Park, *Acc. Chem. Res.*, 2012, **45**, 544.

19 V. V. Shynkar, A. S. Klymchenko, E. Piemont, A. P. Demchenko and Y. Mely, *J. Phys. Chem. A*, 2004, **108**, 8151.

20 K. Sakai, T. Tsuzuki, Y. Itoh, M. Ichikawa and Y. Taniguchi, *Appl. Phys. Lett.*, 2005, **86**, 081103.

21 F. S. Liang, L. X. Wang, D. G. Ma, X. B. Jing and F. S. Wang, *Appl. Phys. Lett.*, 2002, **81**, 4.

22 A. P. Dalmau, *J. Org. Chem.*, 1995, **60**, 5468.

23 D. Y. Chen, C. L. Chen, Y. M. Cheng, C. H. Lai, J. Y. Yu, B. S. Chen, C. C. Hsieh, H. C. Chen, L. Y. Chen, C. Y. Wei, C. C. Wu and P. T. Chou, *ACS Appl. Mater. Interfaces*, 2010, **2**, 1621.

24 A. Z. Weller, *Elektrokhimiya*, 1956, **60**, 1144.

25 (*a*) H. Tong, M. HäuBler, Y. Q. Dong, Z. Li, B. X. Mi, H. S. Kwok and B. Z. Tang, *J. Chin. Chem. Soc.*, 2006, **53**, 243; (*b*) S. Li, L. He, F. Xiong, Y. Li and G. Yang, *J. Phys. Chem. B*, 2004, **108**, 10887; (*c*) X. Chen, R. Wei, Y. Xiang, Z. Zhou, K. Li, P. Song and A. Tong, *J. Phys. Chem. C*, 2011, **115**, 14353.

26 L. Jiang, L. Wang, M. Guo, G. Yin and R. Y. Wang, *Sens. Actuators, B*, 2011, **156**, 825.

27 D. R. Bender, D. Kanne, J. D. Frazier and H. Rapoport, *J. Org. Chem.*, 1983, **16**, 2714.

28 R. Hu, S. Y. Li, Y. Zeng, J. P. Chen, S. Q. Wang, Y. Li and G. Q. Yang, *Phys. Chem. Chem. Phys.*, 2011, **13**, 2044.

29 T. He, X. T. Tao, J. X. Yang, D. Guo, H. B. Xia, J. Jia and M. H. Jiang, *Chem. Commun.*, 2011, **47**, 2907.

30 (*a*) K. Ando, S. Hayashi and S. Kato, *Phys. Chem. Chem. Phys.*, 2011, **13**, 11118; (*b*) C. C. Hsieh, C. M. Jiang and P. T. Chou, *Acc. Chem. Res.*, 2010, **43**, 1364; (*c*) G. Y. Li, G. J. Zhao, Y. H. Liu, K. L. Han and G. Z. He, *J. Comput. Chem.*, 2010, **31**, 1759; (*d*) J. N. Li, M. Pu, D. C. Fang, M. Wei, J. He and D. E. Evans, *J. Mol. Struct.*, 2012, **1015**, 106; (*e*) G. Gui, Z. Lan and W. Thiel, *J. Am. Chem. Soc.*, 2012, **134**, 1662.

31 T. Sekikawa, O. Schalk, G. R. Wu, A. E. Boguslavskiy and A. Stolow, *J. Phys. Chem. A*, 2013, **117**, 2971.

32 X. Cao, X. Zeng, L. Mu, Y. Chen, R. X. Wang, Y. Q. Zhang, J. X. Zhang and G. Wei, *Sens. Actuators, B*, 2013, **177**, 493.